Welding in the World (2018) 62:1285–1300
https://doi.org/10.1007/s40194-018-0657-8

RESEARCH PAPER

Fatigue strength assessment of duplex and super-duplex stainless steels by 4R method

Timo Björk[1] · Heli Mettänen[1] · Antti Ahola[1] · Mari Lindgren[2] · Juuso Terva[3]

Received: 13 September 2017 / Accepted: 24 September 2018 / Published online: 4 October 2018

Abstract

Duplex and super-duplex stainless steels are increasingly used in applications where good fatigue strength is demanded in addition to corrosion resistance. In this research work, the fatigue strength of duplex and super-duplex steels was investigated experimentally, using standard fatigue strength assessment methods, and theoretically, using conventional design methods and a novel effective notch stress-based procedure, the 4R method. The experimental tests included testing of welded joints with and without post-weld treatment. The experimental results were compared with the 4R method. The test results indicated good fatigue strength properties for both materials in the as-welded (ASW) condition, and post-weld treatment by high frequency impact (HFMI)-treatment improved the fatigue resistance at low stress ratios. No improvement, however, was found in the case of high mean stress of the applied load. The results obtained by the theoretical investigation agreed quite well with the experimental results.

Keywords Fatigue · Duplex steels · Super-duplex steels · HFMI · 4R method

1 Introduction

Use of duplex and super-duplex steels has increased greatly due to their good corrosion resistance and advantageous mechanical properties combined with moderate material costs. In addition to corrosion resistance, many applications often require good fatigue strength properties. In the literature, some test results can be found for the fatigue design of welded joints of duplex steels [1–6] but more reliable and consistent fatigue strength data is needed, particularly concerning super-duplex steels. In the present study, an extensive fatigue test program was carried out on welded joints made of duplex 2205 (EN 1.4462) and super-duplex 2507 (EN 1.4410) steel. The investigated materials are used in, e.g., process industries, whose equipment was the specific application area of this research. For this reason, the test specimens in this work were fabricated by an industrial partner.

A number of fundamental questions remain inadequately resolved, which is hindering more widespread use of duplex steels, in particular, issues related to weld quality, mean stress effects due to the presence of residual stresses and as a result of applied load, and fatigue strength improvement potential from post-weld treatment. Current design codes and recommendations [7–11] do not provide fully adequate answers, and an advanced fatigue assessment approach called the 4R method was therefore developed to address these shortcomings. Previously, the method has been applied successfully to butt-welded steel joints in ASW- and post-weld-treated condition [12–14], multiple welded joints under variable amplitude loading [15], and recently, to steel plates with thermally cut edges [16]. In the current project, of which this study forms a part, a new "continuous" S-N curve was obtained for welded joints made of duplex and super-duplex steels. The project also included static tests of welded joints and fatigue tests of cut edges produced using different cutting processes, the results of which will be reported in future work.

Recommended for publication by Commission XIII - Fatigue of Welded Components and Structures

✉ Timo Björk
timo.bjork@lut.fi

[1] Laboratory of Steel Structures, Lappeenranta University of Technology, P.O. Box 20, FI-53851 Lappeenranta, Finland

[2] Outotec Research Center, P.O. Box 69, FI-28101 Pori, Finland

[3] Laboratory of Materials Science, Tampere University of Technology, P.O. Box 589, FI-33101 Tampere, Finland

2 4R method

Current fatigue design rules, e.g., Eurocode 3 and the recommendations by IIW and classification societies [7, 9–11],

provide limited possibilities to consider essential fatigue parameters in terms of material strength, mean stress due to applied load, residual stress from the fabrication processes, and real local joint geometry. In order to eliminate these obstacles, a new fatigue design procedure called the 4R method has been developed [12–15]. The 4R method is based on an effective notch stress (ENS) approach and is applicable to welded joints and cut edges. The underlying principle of the method is based on conversion of available stress range data from experimental tests to local elastic-plastic behavior. The following material and joint data are needed:

- material ultimate strength, $\boldsymbol{R}_m$
- applied stress ratio, $\boldsymbol{R}$
- residual stress, σ_{res}
- weld toe geometrical quality in terms of $\boldsymbol{r}_{\text{true}}$

The letters given in bold ($\boldsymbol{R}$ and $\boldsymbol{r}$) explain the name of the approach—the 4R method. If a joint is loaded by nominal stress range $\Delta\sigma_{\text{nom}}$ as illustrated in Fig. 1, the membrane $\Delta\sigma_m$ and bending stress range $\Delta\sigma_b$ components can be defined based on the type of load, the joint geometry, and the misalignments. The notch stress concentration factors (SCFs) due to the local weld (and joint) geometry are calculated for the membrane ($K_{t,m}$) and bending stress ranges ($K_{t,b}$) separately, as introduced by Ahola et al. [17]. The calculations are carried out using the ENS method and considering the weld quality by adjusting the weld toe radius $r = r_{\text{true}} + 1$ mm. If the weld geometry is smooth, a fillet-type radius can be applied. In the case of undercut, the radius must be modeled by removing material at the weld toe.

The local SCFs can be defined using finite element analyses (FEAs) or available analytical formulas, such as presented e.g., by Ushirokawa and Nakayama [18], Anthes et al. [19] and Brennan et al. [20]. In recent work, Dabiri et al. [21, 22] demonstrated the potential of using an artificial neural network (ANN) procedure to predict SCFs for different types of butt-welded and fillet-welded joints. Once the local SCFs are known, the fatigue notch factor K_f can then be calculated taking into account the notch sensitive parameter q. However, for smooth weld geometries and high strength steels $K_f \approx K_t$. Thus, the local notch stress (ENS) σ_k is:

$$\sigma_k = K_f \sigma_{nom} \approx K_t \sigma_{\text{nom}} = K_{t,m}\sigma_m + K_{t,b}\sigma_b \tag{1}$$

Conventionally, the stress ratio due to applied load is defined based on nominal stresses:

$$R = \frac{\sigma_{\text{hs,min}}}{\sigma_{\text{hs},max}} = \frac{\sigma_{k,\text{min}}}{\sigma_{k,\text{max}}} \approx \frac{\sigma_{\text{nom,min}}}{\sigma_{\text{nom,max}}} \tag{2}$$

where σ_{hs} is structural (hot spot) stress. However, in the case of geometrical nonlinear stress behavior, for instance, due to buckling or angular misalignment of the joint under the membrane loading, the structural (hot spot) stress or local notch stress is a more rigorous approach to define the stress ratio of the applied load.

The main idea of the 4R method (previously termed the 3R method since r_{true} was not included) is to estimate the fatigue strength of the joint or cut surface based on the material's cyclic elastic-plastic behavior at a notch as illustrated in Fig. 2.

The material stress-strain (σ-ε) behavior can be described by means of the Ramberg-Osgood (R-O) material model:

$$\varepsilon = \frac{\sigma}{E} + \left(\frac{\sigma}{H}\right)^{\frac{1}{n}}, \tag{3}$$

where E is Young's modulus, n is an elastic-plastic strain hardening exponent, and H is the strength coefficient. The local residual stresses σ_{res} can be positive, for instance, in the as-welded (ASW) condition, or compressive, for example,

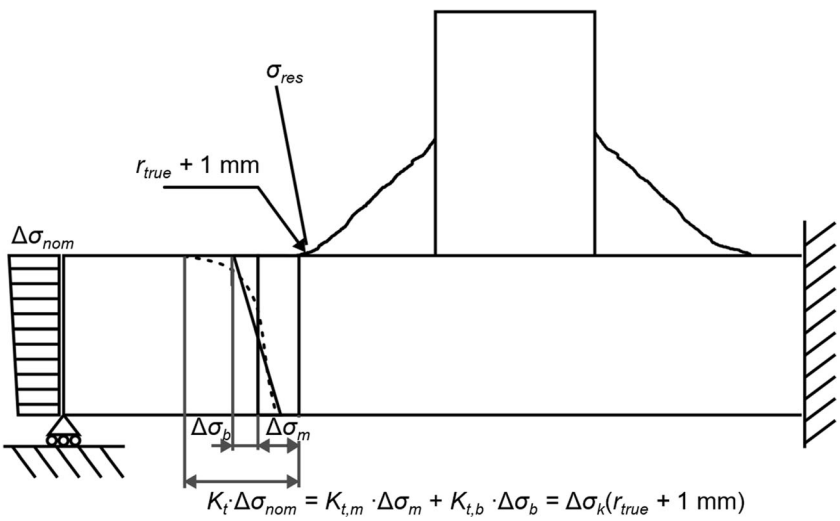

Fig. 1 Stresses needed for the 4R approach

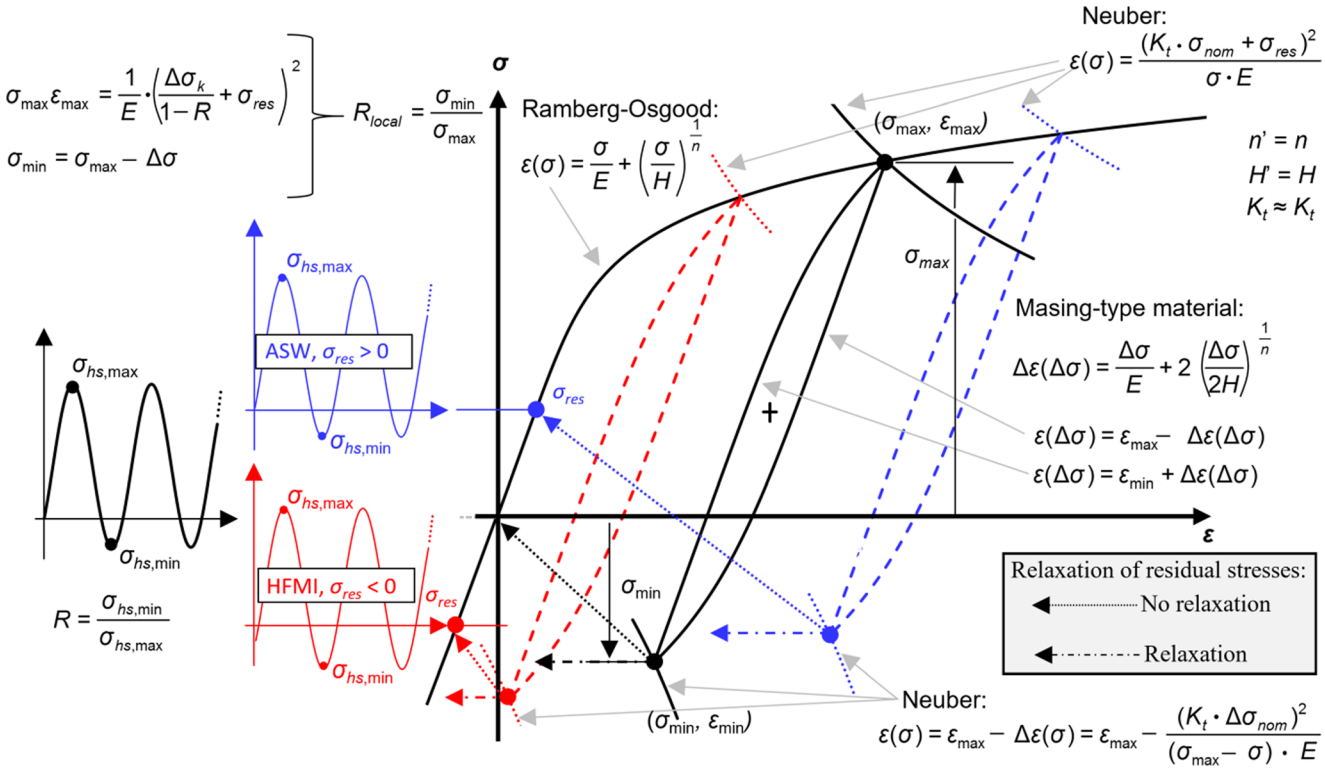

Fig. 2 Principles to define R_{local} for the master curve of the 4R approach

due to post-weld treatments such as high frequency mechanical impact (HFMI) treatment. The elastic-plastic stress-strain behavior considers the effect of residual stresses and is controlled by Neuber's rule described by the well-known Neuber hyperbola [23], which in this case can be written:

$$\varepsilon\sigma = \frac{(K_t\sigma_{\text{nom}} + \sigma_{\text{res}})^2}{E} = \frac{(\sigma_k + \sigma_{\text{res}})^2}{E} \tag{4}$$

Considering the mean stress effect according to the Smith-Watson-Topper (SWT) approach, the maximum values for stress and strain can be obtained:

$$\varepsilon_{\max}\sigma_{\max} = \frac{\left(\frac{\Delta\sigma_k}{1-R} + \sigma_{res}\right)^2}{E} \tag{5}$$

The turning point (= $\sigma_{\max}$, $\varepsilon_{\max}$) of the cyclic material behavior can be calculated from Eqs. (3) and (5). In accordance with the unloading phase, strain decreases, and follows the Masing equation [24]:

$$\Delta\varepsilon = \frac{\Delta\sigma}{E} + 2\left(\frac{\Delta\sigma}{2H}\right)^{\frac{1}{n}} \tag{6}$$

The hysteresis loop reaches its lower turning point when the stress-strain curve approaches the lower branch of the Neuber hyperbola:

$$\Delta\varepsilon\Delta\sigma = \frac{(\Delta\sigma_k)^2}{E} \tag{7}$$

Now, the minimum values (= $\sigma_{\min}$, $\varepsilon_{\min}$) can be calculated, and the key parameter, the local stress ratio, can be obtained:

$$R_{local} = \frac{\sigma_{\min}}{\sigma_{\max}} = 1 - \frac{\Delta\sigma}{\sigma_{\max}} \tag{8}$$

By setting $R_{\text{local,ref}} = 0$, a local reference coordinate system can be established where the data points ($\Delta\sigma_{k,i}$ and $N_{f,i}$ from experimental tests) can be converted to stress ranges in a local reference coordinate system using the SWT-approach:

$$\Delta\sigma_{k,ref,i} = \Delta\sigma_{k,i}\frac{\sqrt{1-R_{local,ref}}}{\sqrt{1-R_{local}}} = \frac{\Delta\sigma_{k,i}}{\sqrt{1-R_{local}}} \tag{9}$$

Conventionally, in the statistical analysis of S-N curves, it is assumed that stress range is unambiguously known, i.e., stress range is independent variable, and the scatter in number of cycles (dependent variable) is solely considered. Nevertheless, due to the high variation e.g., in specimen

shape, weld reinforcement and toe geometry, and residual stresses, unambiguity of true acting stress range in a test describing the S-N behavior can be highly questionable. Consequently, a master curve of the 4R method is established considering the scatter in both stress range and number of cycles. Nykänen et al. [13] has shown that use of this approach leads to higher correlation coefficient (R^2) than conventional regression analysis also for other stress-based approaches than the 4R method. This procedure provides the optimal estimation of the relationship between stress range and fatigue life. The master curve passes the mass center of the data point cloud and the slope m fixes the axis to minimize the inertia of the data point, as illustrated in Fig. 3. This results in:

$$m = \frac{\sum v_i^2 - \sum u_i^2 \pm \sqrt{\left(\sum v_i^2 - \sum u_i^2\right)^2 + 4\sum (v_i u_i)^2}}{2\sum v_i u_i} \tag{10}$$

where:

$$u_i = \log\Delta\sigma_{k,\mathrm{ref},i} - \frac{\sum_{j=1}^{n} \log\Delta\sigma_{k,\mathrm{ref},j}}{n} \quad \text{and} \quad v_i = \log N_{f,i} - \frac{\sum_{j=1}^{n} \log N_{f,j}}{n} \tag{11}$$

The constant of S-N curve will be:

$$\log C_{\mathrm{mean}} = \frac{\sum\left(\log N_{f,i} - m\log\Delta\sigma_{k,\mathrm{ref},i}\right)}{n} \quad \text{and} \quad \log C_{char} = C_{\mathrm{mean}} - k_1 \cdot Stdv \tag{12}$$

where k_1 is a multiplication factor depending on the number of data points and is available in the IIW recommendations [9].

This application of Deming's regression [25] to fit S-N curve can be alternatively used if the scatter of stress ranges and cycles can be assumed to have the same distribution form. This is a fundamental principle because regardless of the analyzing method the effective stress range always has large scatter and cannot be defined unambiguously. Consequently, an approach using minimization of the sum of squared perpendicular distances (=MSSPD), Fig. 3, is physically logical and improves the accuracy of the fatigue prediction [13].

Utilizing the above curve fitting approach, Nykänen et al. [13] analyzed a large number of test results and fitted the constants C and m for his new 4R master curve. Unfortunately, the fatigue test data used by Nykänen et al. does not include all the essential parameters needed for the 4R method, which is understandable since the earlier tests were not carried out for the kind of local stress approaches considered in the current work. The S-N curve is a basic reference design curve that is independent of the steel grade and is valid for $R_{\mathrm{local,\ ref}} = 0$ with the constants $m = 5.85$ and $C_{\mathrm{mean}} = 10^{21.59}$ and $C_{\mathrm{char}} = 10^{20.83}$. New design curves can be created by considering the real steel grade, R_m, based on the nominal classification value of the steel (design phase), material certification (pre-fabrication phase), or measured hardness values (after the manufacturing phase). The new

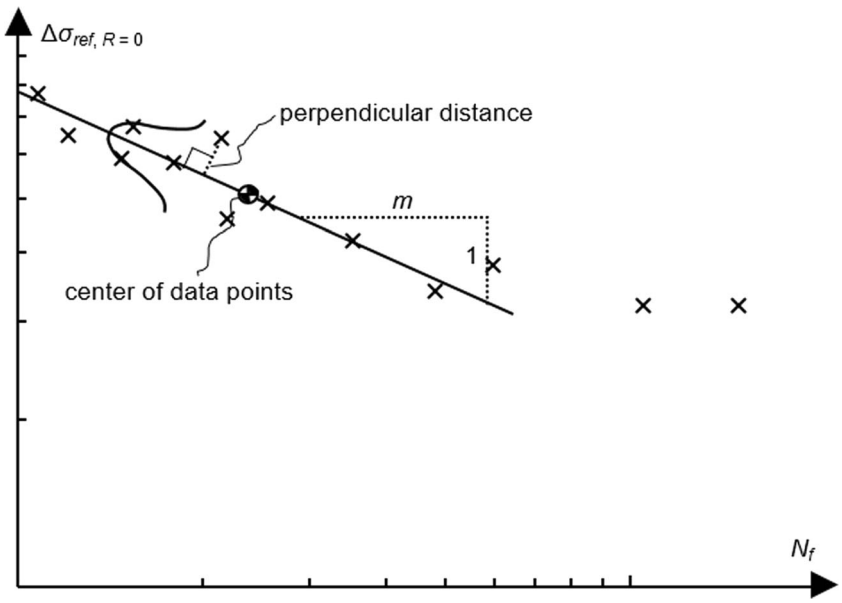

Fig. 3 Defining the best possible S-N correlation by the minimization of the sum of squared perpendicular distances (MSSPD)

design curve thus takes into account the real local stress ratio effect, R_{local}, which depends on the material (R_m), the R value of the applied load, and the residual stresses (σ_{res}). The residual stresses can be estimated by using default values for ASW- or HFMI-treated joints, as presented in [14], or by using measured values. Additionally, definition of the local joint geometry can be based on the design assumptions or measured values, depending on the phase of analyzing process. Figure 4 gives the principles for the analysis process of the 4R method in the different analysis phases. Considering the parameters of the 4R method, the reference master curve can now be converted to new continuous S-N curves and used to estimate the fatigue life:

$$N_f = \frac{C_{ref}}{\left(\sqrt{1-R_{local}}\Delta\sigma_k\right)^m} \tag{13}$$

where C_{ref} is either the mean or characteristic value from Eq. (12).

In a normal design case, existing continuous fatigue curves of the 4R method can be applied directly or a new tuned curve can be created from experimental results, if the critical parameters are measured or otherwise available, Fig. 4. In this paper, a new master curve is defined by means of the following principles:

- material parameters: $E = 200$ GPa, $n = 0.15$, $H = 1.65 \cdot R_m$, where R_m is obtained from the material specification
- original data points ($\Delta\sigma_{m,i}$, $\Delta\sigma_{b,i}$, and $N_{f,i}$), obtained from constant amplitude fatigue tests based on measured geometries and strain gage values.

  SCFs $K_{t,m}$ and $K_{t,b}$ defined by FEA, using $r = 1$ mm for ASW- and HFMI-treated specimens
- residual stresses σ_{res}, measured by X-ray and also by using the default value, i.e., $\sigma_{res} = -0.255 \cdot R_m$ for HFMI-treated specimens as introduced in [14].

3 Experimental program

3.1 Materials

The duplex steel specimens (2205) were manufactured from hot-rolled $t = 5$-mm sheets and super-duplex steel specimens (2507) from $t = 5$-mm cold-rolled sheets. The filler materials for the 2205 and 2507 welded joints were Ø1.2 mm Cromacore DW 329A and Tetra S D57L-G, respectively. The chemical compositions and mechanical properties of the parent and filler materials are shown in Tables 1 and 2.

3.2 Test specimens

A total of 63 different welded specimens were manufactured and tested to obtain the fatigue strength properties of duplex and super-duplex joints. The test program included both ASW- and HFMI-treated welded joints as shown in Table 3. The main dimensions of the specimens are illustrated in Fig. 5. Only HFMI was applied as a post-weld treatment method in this investigation, because TIG dressing will change the balance of chemical compositions and thus might result in decreased corrosion resistance, and burr grinding is not a desirable process in most applications. The HFMI treatment was conducted using the commercial DYNATEC device (model HFM 12 P1) distributed by PFEIFER [29], and following the general instructions with visual inspections on notch groove (see e.g., Fig. 10c) introduced in [30].

The welded joints were manufactured using a single-pass manual gas metal arc welding (GMAW) process. A partner company with multiple welders fabricated the specimens, and the welding quality thus represents normal workshop quality. The welding parameters and sequence of welds for the fillet welded and butt-welded joints are presented in Table 4 and Fig. 6. Maximum interpass temperature was 150 °C. Weld

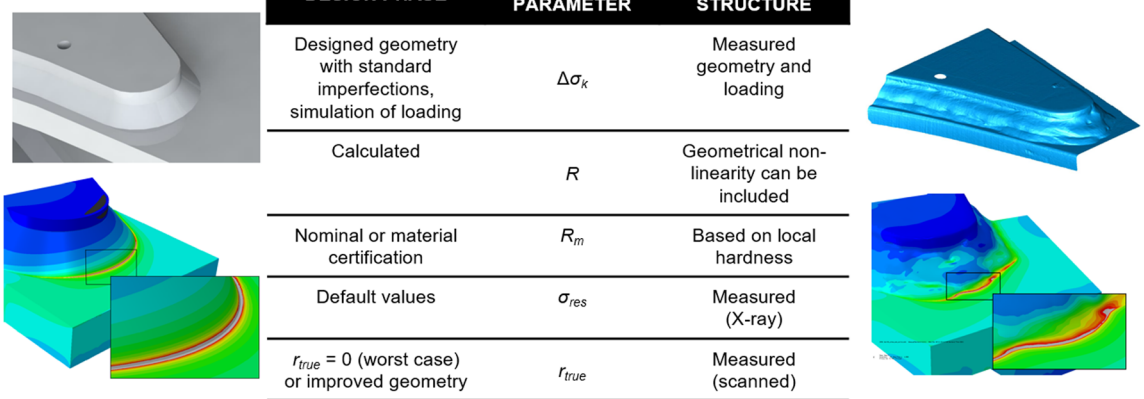

Fig. 4 Parameters in the fatigue assessment of welded structure using the 4R method depending on the analysis phase

Table 1 Chemical composition [weight-%]. Values for the parent materials are from material certificates and for the filler materials are typical values given by the manufacturer

Material	Set	C	Si	Mn	P	S	Cr	Ni	Mo	Cu	Nb	Co	N
2205	–	0.015	0.39	1.34	0.025	0.001	22.59	5.79	3.24	0.25	0.01	0.13	0.179
Cromacore DW 329A [26]	–	0.02	0.8	1.3	–	–	22.9	9.2	3.0	–	–	–	0.1
2507	1	0.015	0.39	0.83	0.024	0.001	25.02	6.94	3.80	0.34	–	–	0.277
2507	2	0.016	0.40	0.85	0.030	0.001	25.26	6.83	3.79	0.37	–	–	0.281
Tetra S D57L-G [27]	–	0.03	0.6	1.4	0.015	0.008	25.0	9.0	3.8	1.0	–	–	–

Table 2 Mechanical properties at room temperature

Material	Type	Proof strength		Tensile strength	Elongation	Hardness
		$R_{p.0.2}$ [MPa]	$R_{p.1.0}$ [MPa]	R_m [MPa]	A_5 [%]	*HB*
2205	Typical [28]	630	–	840	30	270
2205	Measured	625	716	837	31	260
Cromacore DW 329A	Typical [26]	610	–	800	32	–
2507	Typical [28]	730	–	940	24	–
2507	Measured	712	801	917	29	281
Tetra S D57L-G	Typical [27]	830	–	950	22	–

Table 3 Fatigue test program: specimens and test conditions. BJ signifies butt-welded joint, NLCX non-load-carrying X-joint and LCX load-carrying X-joint (see Fig. 5)

Material	Specimen type	Condition	No. of specimens	Specimen IDs
2205	BJ	ASW	10	O5BL01- O5BL10
	BJ	HFMI	5	O5BL11- O5BL15
	NLCX	ASW	10	O5XL01- O5XL10
	NLCX	HFMI	8	O5XL10- O5XL18
2507	BJ	ASW	6	SDBW1- SDBW6
	BJ	HFMI	6	SDBW1H- SDBW6H
	NLCX	ASW	6	SDNL1- SDNL6
	NLCX	HFMI	6	SDNL1H- SDNL6H
	LCX	ASW	6	SDL11-SDL16

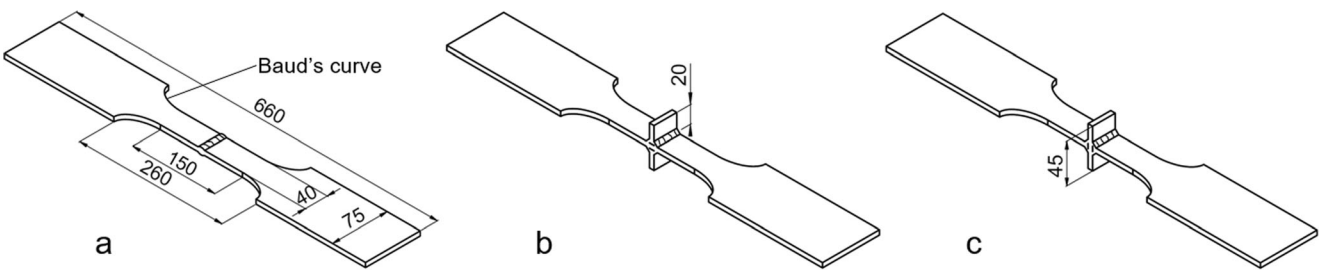

Fig. 5 Test specimens: **a** BJ, **b** NLCX, and **c** LCX

Table 4 Key parameters of the welding procedure specification

Specimen type	Run no.	Current I [A]	Voltage U [V]	Travel speed v [mm/min]	Heat input Q [kJ/mm]
BJ	1	170–210	26–28	220–320	0.8–1.0
	2	190–220	26–29	220–320	0.8–1.0
NLCX and LCX	1–4	190–220	28–31	220–350	0.8–1.0

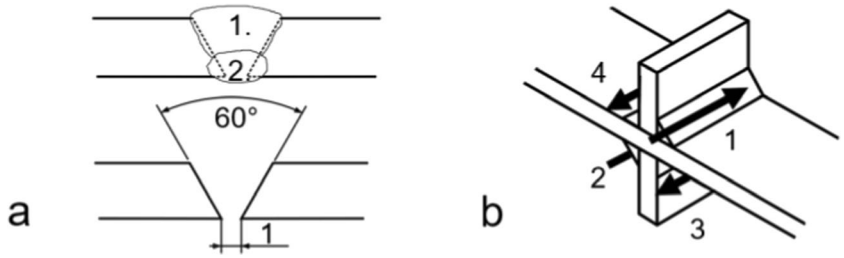

Fig. 6 Sequence of welds: **a** butt-welded joints and **b** fillet-welded X-joints (arrows present the welding direction)

start and stop positions were subsequently sawed and machined, and the sheet edges were ground to avoid fatigue failures starting from the edge (see Fig. 7).

Residual stresses were measured with X-ray diffraction from the surface of the specimens along the loading direction. For the NLC X-joints made of 2507 steel, an example of residual stress distribution is presented in Fig. 8. In the ASW specimen, the residual stresses were close to zero, i.e., the maximum value of four weld toes. In particular, in the HFMI-treated joints, beneficial compressive residual stresses were obtained at each weld toe. More detailed descriptions and results of measurements can be found in [31, 32].

The microstructure of the specimens was investigated with a Zeiss Axio Observer optical microscope. Hardness and microhardness measurements were carried out with Struers DuraScan hardness testing equipment using 5 kg and 100 g loads. Figure 9 presents the microhardnesses of ASW- and HFMI-treated specimens. Selected fracture surfaces were characterized using a Jeol JSM 6490 LV scanning electron microscope.

3.3 Test setup

All specimens were subjected to fluctuating tensile loading (Fig. 10d) and, consequently, the loading was mainly membrane stress. Bending stress existed only as a secondary component due to angular misalignment and plate offset. Each specimen was equipped with a strain gage at $0.4t$ distance from the weld toe to measure the hot spot stress (Fig. 10a, b). The structural SCFs were low; the average for all the specimens was $k_{m,\mathrm{mean}} = 1.18$. Nevertheless, it is important to measure the real structural stress ranges using strain gages and to identify the geometrical nonlinearities. In addition, the clamping effect was measured, but because of the straightness of the specimens, the ENSs due to fixing into the loading rig were rather small, in all cases under 110 MPa.

4 Finite element analyses

FEA was carried out to obtain the elastic SCF for each test. The height and width of weld reinforcement were measured in

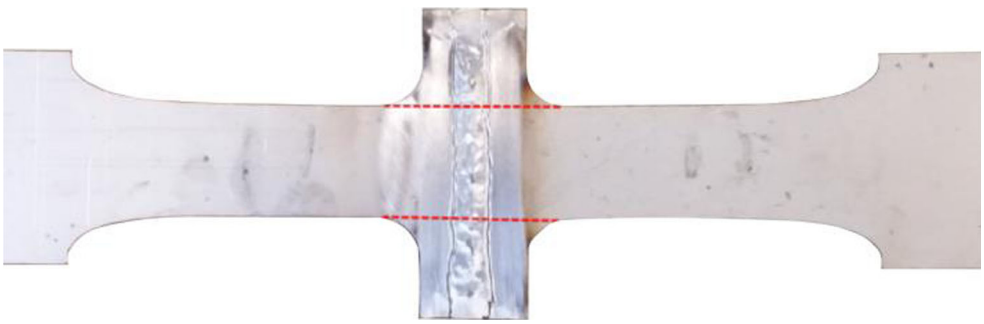

Fig. 7 A butt-welded and HFMI-treated specimen before machining

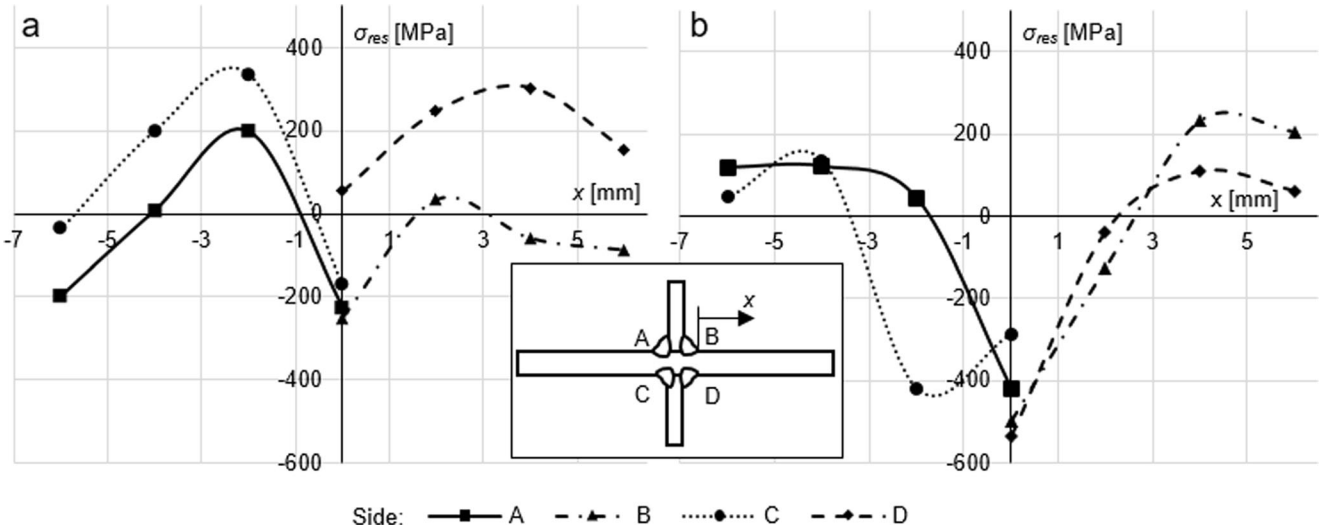

Fig. 8 Residual stress distribution along the surface in NLC X-joints: **a** ASW- and **b** HFMI-treated conditions

the butt-welded specimens, and the flank angle and throat thickness in the fillet welded specimens, respectively. In the butt-welded joints, an arc with dimensions of w and h were modeled (Fig. 11b), and in the fillet welded joints, idealized straight-line welds, (Fig. 11a), were modeled by means of two-dimensional shape laser measurements. In the FEAs, a weld toe radius $r = 1$ mm was assumed regardless of the test condition, i.e., ASW- or HFMI-treated, since $r = 1$ mm has been discovered to be applicable also for post-weld treated joints [12, 14, 33].

SCFs, $K_{t,i}$, were obtained using linear static analysis with a nominal seed loading of 1 MPa. Pre- and post-processing were performed using Femap (Siemens PLM Software), and the FE-models were analyzed with NX Nastran (Siemens PLM

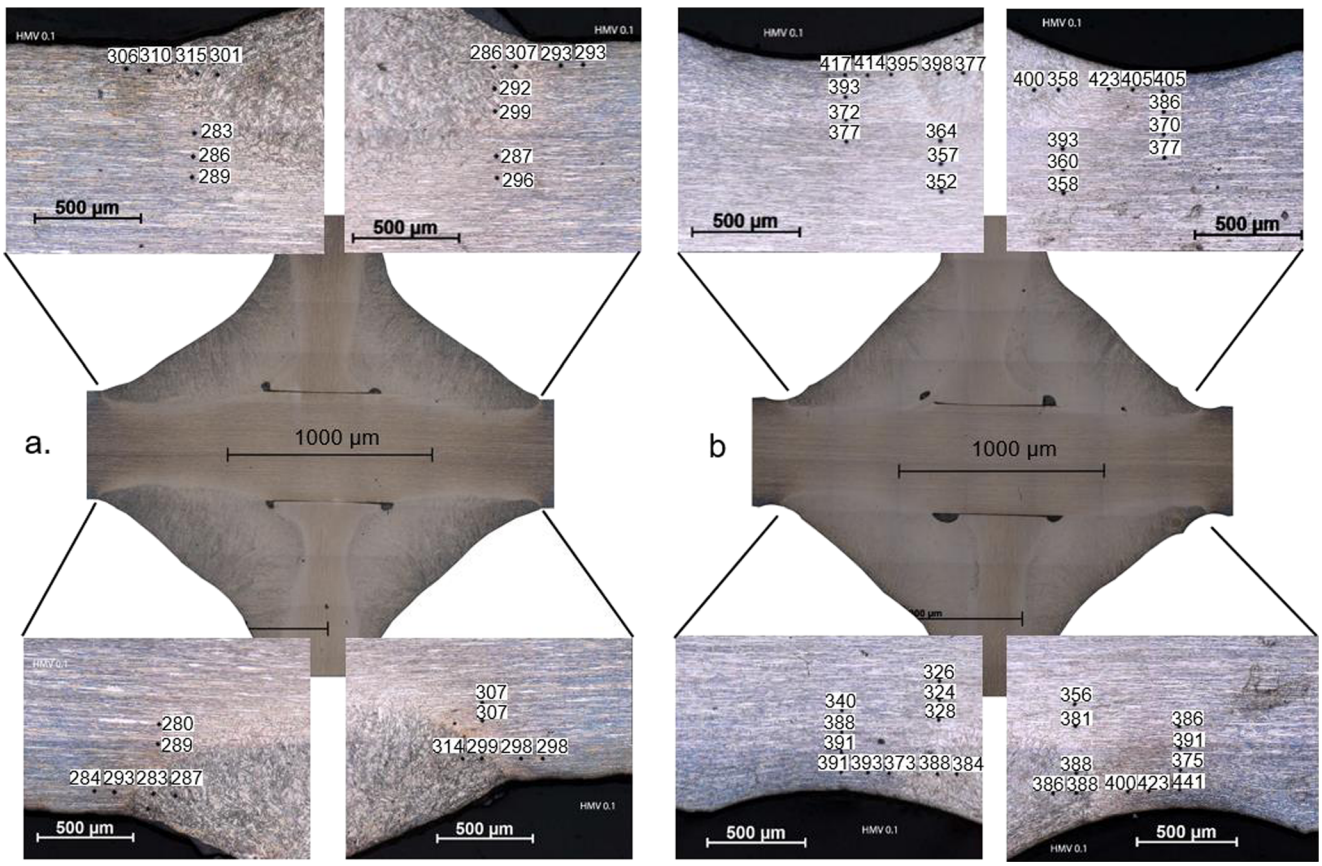

Fig. 9 Microhardnesses at the weld toes: **a** ASW- and **b** HFMI-treated NLCX specimens

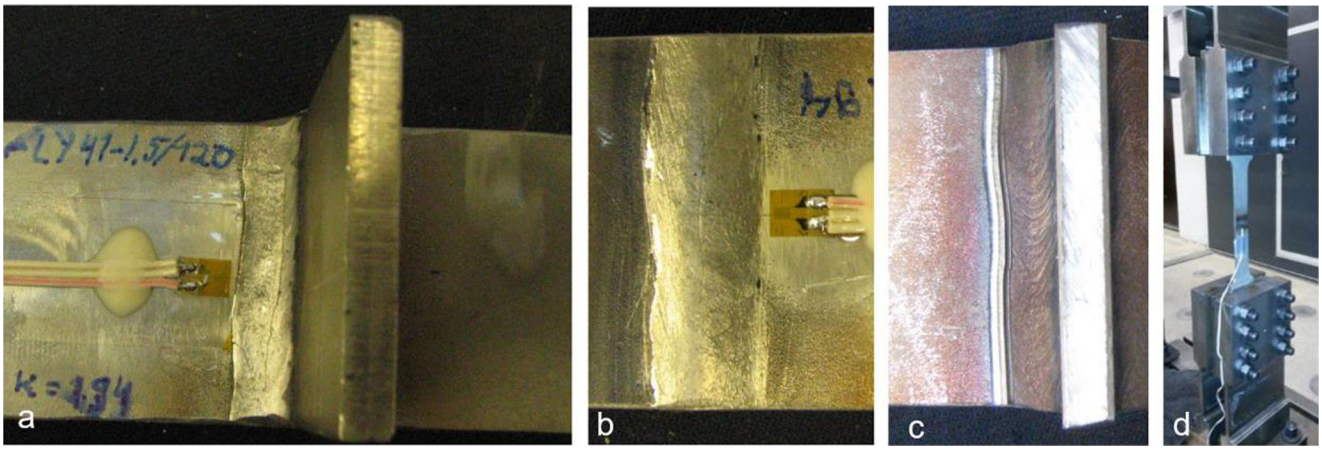

Fig. 10 BJ and NLCX specimens in the **a**, **b** ASW- and **c** HFMI-treated condition, and **d** test rig

Software). The models were meshed with quadratic quadrilateral 8-node plane strain elements (see Fig. 11). At the weld toes, a dense, and regular mesh shape was applied, i.e., aspect ratio 1:2 and 16 elements at an arc. Due to symmetry, only one half was modeled and symmetry boundary conditions were applied. Neither weld imperfections nor plate or angular misalignments causing secondary bending stresses were modeled. Alternatively, the membrane and bending stress for each test were measured by means of a strain gage, and the stress components were multiplied by the SCFs $K_{t,m}$ and $K_{t,b}$ to obtain the ENS.

5 Results

5.1 Conventional S-N approaches

In nine specimens, the fatigue failure did not occur in the area under investigation, e.g., in some HFMI-treated BJ specimens, the fatigue failure occurred at the ground sheet edge. These results were excluded from the studied data when the fatigue strengths of each joint type were determined. The mean fatigue strengths (50% survival probability) were obtained using the standard procedure as follows:

$$\log N_f = \log C - m \cdot \log \Delta\sigma, \tag{14}$$

where N_f is number of cycles (dependent variable), C fatigue capacity, m slope of the S-N curve, and $\Delta\sigma$ stress range (independent variable). Additionally, the test results were compared with the fatigue strengths of each joint given by the IIW recommendations [9]. The mean curves for each category were obtained using a safety factor of $j_\sigma = 1.37$ [34]. For the ENS method, $FAT_{50\%} = 309$ MPa has been verified also by test results [13]. The test results are plotted in Figs. 12 and 13 for the different fatigue assessment approaches, and Table 5 summarizes the obtained fatigue strengths.

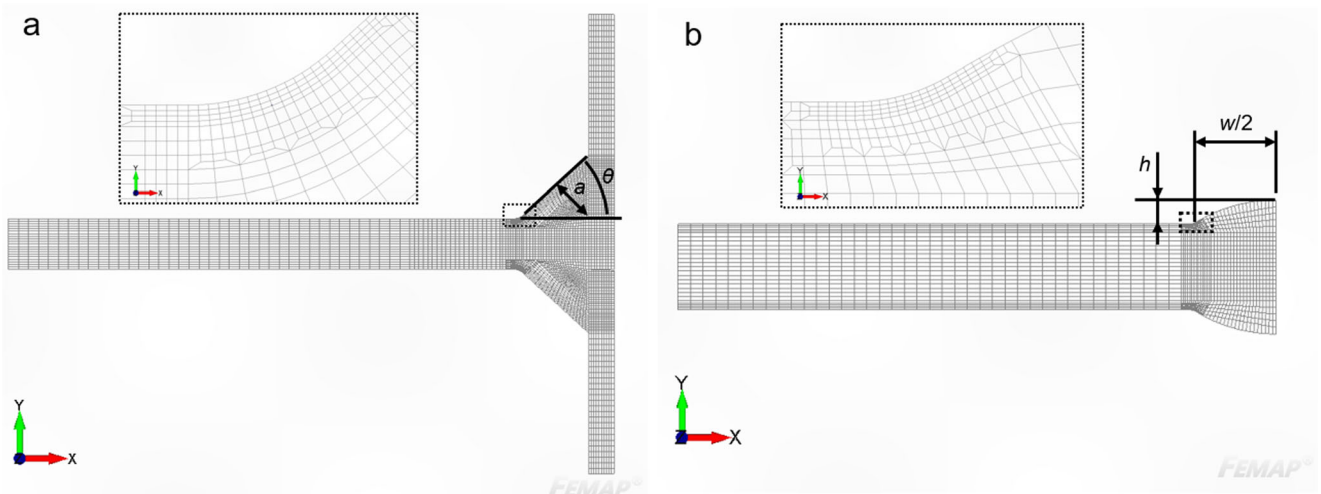

Fig. 11 Typical meshes: **a** NLCX and **b** BJ models

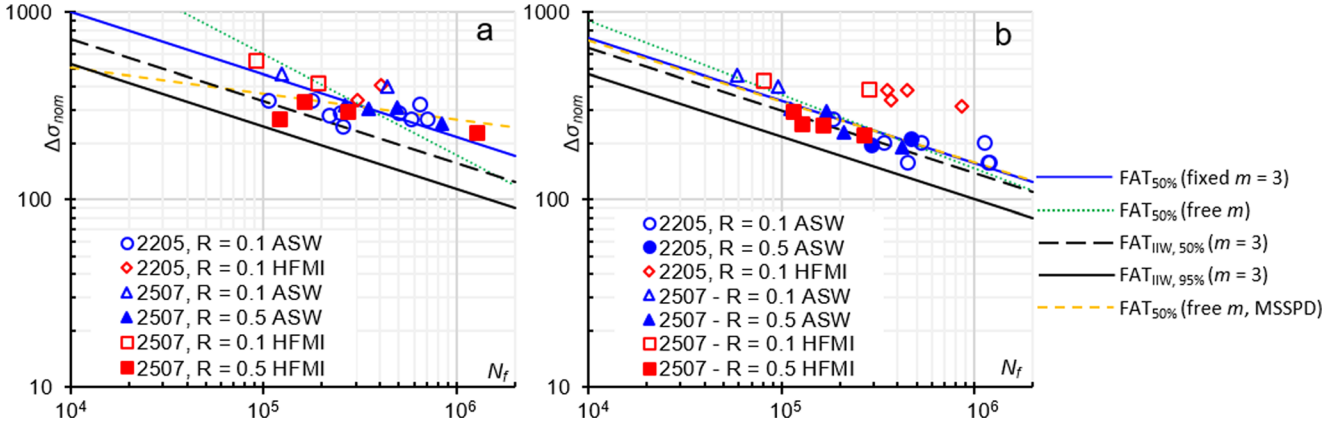

Fig. 12 Test results of **a** BJ and **b** NLCX specimens in terms of the nominal stress system

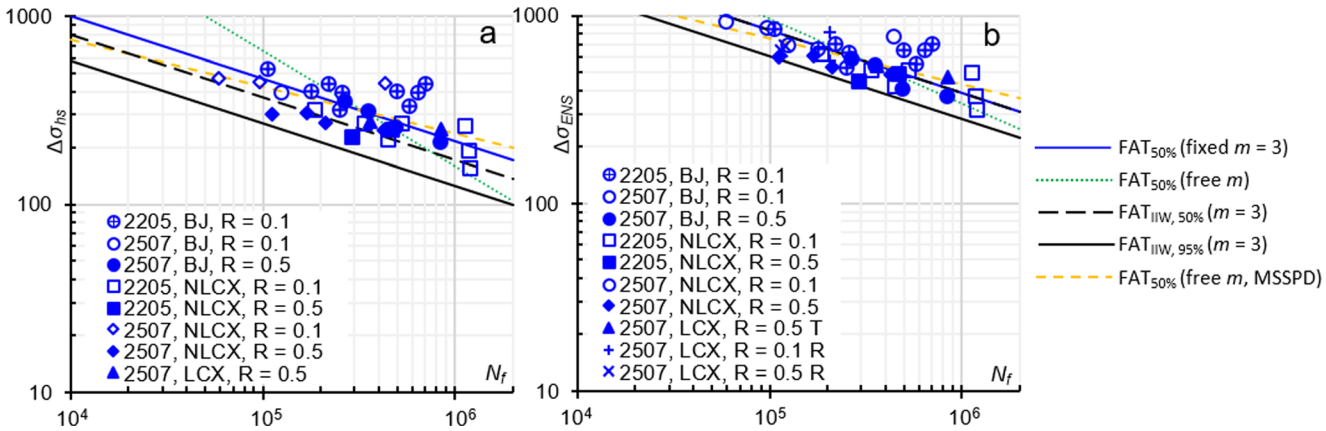

Fig. 13 ASW test results of welded details in terms of (**a**) structural HS stress and (**b**) ENS system

There was no major difference between fatigue strengths of ASW specimens tested at $R = 0.1$ and $R = 0.5$ external stress ratios within this test series, as Fig. 12 introduces. In particular, in the HFMI-treated joints made of 2507, a distinct decrease in fatigue strength was found when higher stress ratio was applied. In HFMI-treated joints made of 2205, the lower applied stress ratio ($R = 0.1$ with respect to $R = 0.5$), or HFMI treatment with respect to the joints in ASW condition, did not result in higher fatigue strength. Due to these aforementioned issues, all data points (ASW and HFMI, as well as $R = 0.1$ and $R = 0.5$ joints) were included in the same regression analyses used for obtaining fatigue strengths. Figure 13 presents the fatigue strengths of all welded joints in the ASW condition ascertained with the structural HS approach and the ENS approach. The exact FAT values and S-N slopes are presented in Table 5.

Table 5 Nominal fatigue strengths [MPa] for the welded details in ASW condition in comparison with IIW values. Indices indicates the survival probability (mean 50% or characteristic 97.7%)

	IIW values		Test results				
	$m = 3$		$m = 3$	Free m			
			Standard procedure			MSSPD	
Specimen type	$FAT_{97.7\%}$	$FAT_{50\%}$	$FAT_{50\%}$	m	$FAT_{50\%}$	m	$FAT_{50\%}$
Nom—BJ	90	123	171	1.86	118	7.10	241
Nom—NLCX	80	110	124	2.53	111	3.07	126
HS—All joints	100*	137	173	1.62	104	4.00	200
ENS—All joints	225	309	309	2.21	247	4.12	366

* Excluding LCX joint type which $FAT_{97.7\%} = 90$ MPa

The elastic SCFs (K_t) were determined for each joint by means of FEA to obtain the fatigue strengths with the ENS and 4R methods. The finite element analyses are described more comprehensively in Section 4. When considering the local approaches of the welded joints, the HS method seems to be conservative, since the obtained mean curve (FAT = 173 MPa, $m = 3$) is 26% higher than the computed mean curve (FAT = 137 MPa). In particular, the derived mean curve of the ENS approach (FAT = 309 MPa, $m = 3$) equals the computational curve (see Table 5).

5.2 4R method

The structural stress level data points from experimental tests (Table 3) were converted first to ENS level S-N values (Eq. (1)) and then further to the reference coordinate system data points, where $R_{\text{local, ref}} = 0$ (Eqs. 2–12). These results are presented in Fig. 14.

The results from the ASW specimens for both materials were then reanalyzed considering the effect of stress ratio ($R = 0.1$ and $R = 0.5$) due to applied load. The points in Fig.15 are from experimental results and the curves are S-N estimations from Eq. (13). The upper curves refer to minimum residual stress levels and the lower to maximum residual stress, respectively.

The effects of weld post treatment by HFMI on fatigue strength are seen in Fig. 16. The results were separated into two groups depending on the applied stress ratio ($R = 0.1$ and $R = 0.5$). The estimation curves are based on the default value for residual stresses with $\sigma_{\text{res}} = -0.255R_m$ [14], which agree quite well with the measured values.

6 Discussion

The results show that the fatigue strength of welded joints of both investigated materials is good. This is mainly because weld quality is at least moderate (fulfilling the requirements set in ISO 5718 for weld class C). The conventional design methods (nominal, HS, and ENS) match quite well with experimental results, at least with respect to the worst cases (Figs. 12 and 13). However, they do not provide any possibilities to utilize the available better quality influenced by improved geometry, metallurgy or beneficial residual stresses. Consequently, application of the 4R method can be considered justifiable.

The reference master curve defined by the 4R method for the studied duplex and super-duplex steels matches surprisingly well with results from Nykänen et al.'s previous investigations. The results from Fig. 14 give the characteristic FAT class in the reference coordinate system ($R_{\text{local, ref}} = 0$) for these materials as:

$$FAT_{\text{ref},char} = \sqrt[m]{\frac{C_{\text{ref},char}}{2{\cdot}10^6}} = \sqrt[5.83]{\frac{10^{20.96}}{2{\cdot}10^6}} = 327\ \text{MPa} \qquad (15)$$

This is a reasonable result for this kind of high strength steel referring to the results found in the previous studies [12, 14]. In Fig. 17, the test results and calculated fatigue lives are compared in terms of the conventional S-N approaches and 4R method. Figure 17 shows that the 4R method gives reasonable estimation of fatigue life in duplex and super-duplex steels although it is not as efficient as it has been for other materials [12–14].

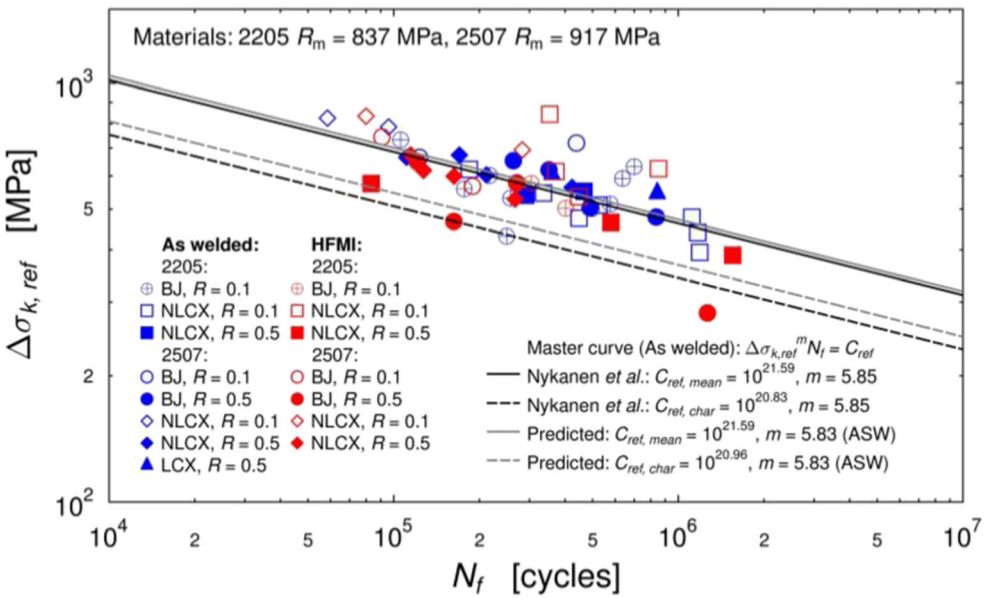

Fig. 14 Data points in the reference coordinate system, $R_{\text{local, ref}} = 0$

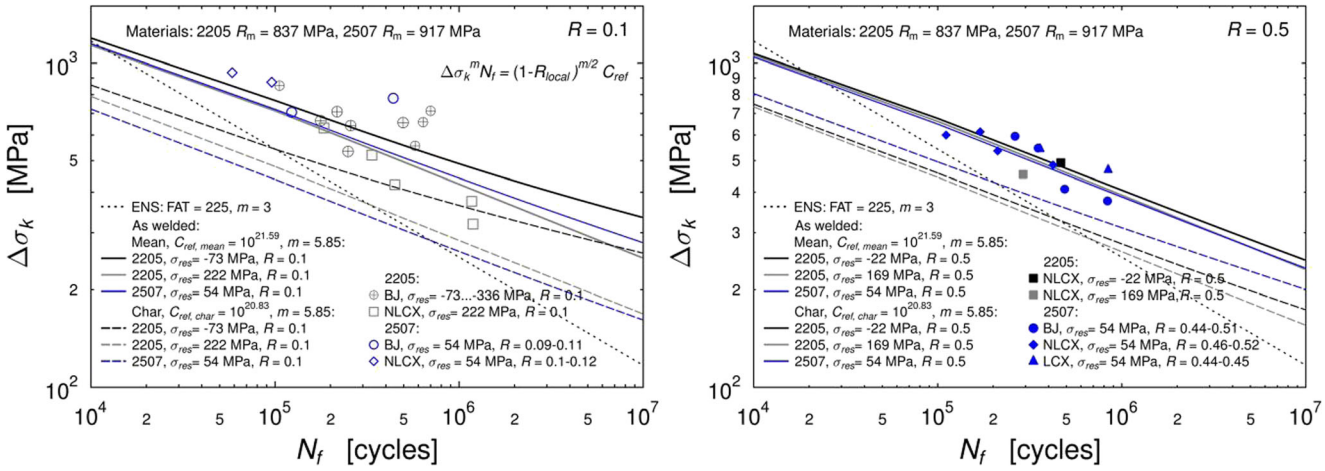

Fig. 15 Continuous S-N curves for the ASW joints for **a** $R = 0.1$ and **b** $R = 0.5$

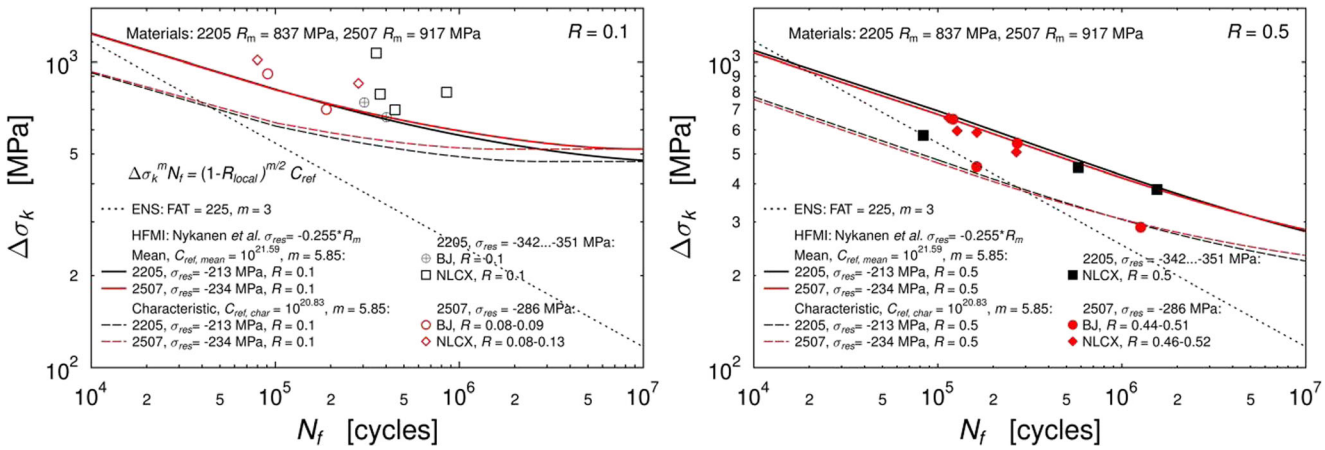

Fig. 16 Continuous S-N curves for the HFMI-treated joints for **a** $R = 0.1$ and **b** $R = 0.5$

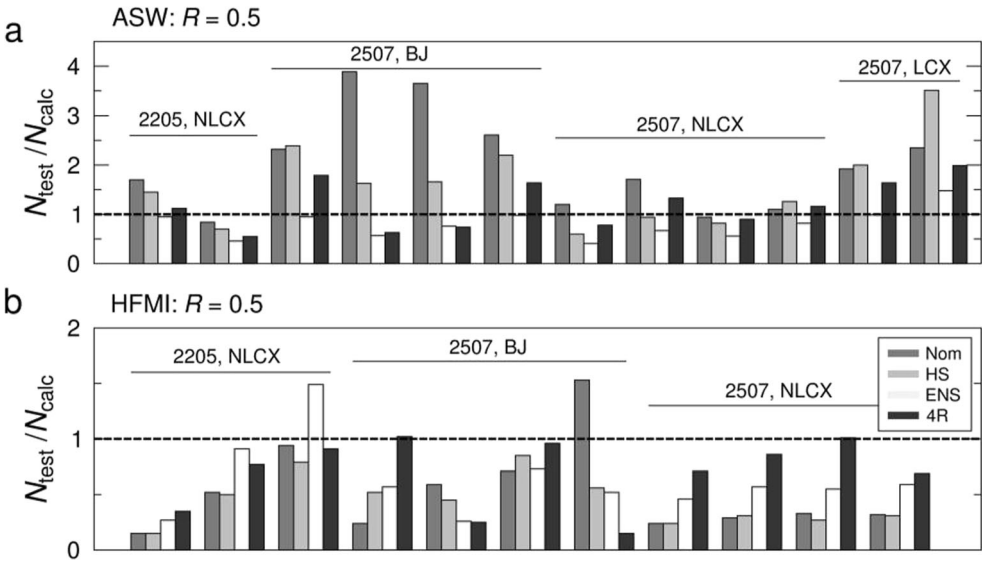

Fig. 17 Test results in comparison with calculated fatigue lives using different fatigue assessment approaches

Within this study, no significant difference in the fatigue strength was found between the $R = 0.1$ and $R = 0.5$ tests (see Figs. 12 and 13). Nevertheless, the previous studies on the applications of 4R method for C-Mn structural steels [12–14], along with many fundamental works [34–36], have shown the importance of consideration of applied stress ratio in the fatigue strength assessment. The 4R method predicts the effects of the stress ratio R and residual stresses σ_{res} due to welding or post treatment directly without any multistep correction procedures. The approach is based not only on regression analyses of the experimental results but also on well-known fatigue theories, such as presented by Radaj, Ramberg-Osgood, Neuber, SWT, and Masing. Instead of using a local strain approach, the reference master S-N curve is, however, still based on experimental results, which utilize fabrication quality and scatter better than material based S-N curves. Consequently, the 4R approach ensures safer use for new applications but also takes important effects, such as stress ratio and residual stresses into account efficiently.

In the case of $R = 0.1$ loading, reasonably high scatter in the test results was obtained (see Fig. 15a). The fatigue strength prediction following the 4R method is sensitive to the residual stress assumption at low stress ratios, since residual stress has direct influence on the local stress ratio R_{local} at notch root. This issue can be seen in Fig. 15a in terms of different S-N curves obtained for different residual stress assumptions. Increasing mean stress level of the applied load, e.g., $R = 0.5$, diminishes the influence of residual stresses on the fatigue strength estimation since local plastic behavior is received also at low stress ranges. Consequently, low scatter was received in the case of $R = 0.5$ loading (see Fig. 15b). Consequently, more detailed and specimen-specific measurements on the residual stresses in the ASW condition within the test series, would have improved the fatigue strength estimation and decreased the scatter of test results in the $R = 0.1$ loading.

The applied stress ratio R has (or has not) an influence on the fatigue strength capacity of welded components depending on the residual stress level and applied stress range with respect to ultimate strength of material ($\Delta\sigma_k/R_m$). For instance, in joints in the ASW condition with high residual stresses, mean stress level of applied load, i.e., applied stress ratio, does not affect substantially on the local stress ratio R_{local} since mean stress level is high due to the high residual stress. However, in the case of low or even compressive residual stress, e.g., due to post-weld treatment, applied stress ratio affects directly on the local stress ratio and subsequently, on the fatigue strength capacity.

HFMI treatment seems to improve the fatigue strength better than the method predicts when the R ratio is low (Fig. 16a), but the situation is rather different with the higher R ratio (Fig. 16b). Although the HFMI treatment improves the fatigue strength, the degree of improvement is lower compared to C-Mn structural steels with the same strength properties, primarily due to metallurgical reasons. Stress gage measurements (Fig. 18) revealed that relaxation occurred under cyclic loading, especially in high mean stresses. Loss of compressive residual stresses due to the relaxation can be one reason for the decrease in the improvement level of the HFMI treatment. Nevertheless, since the master curve is obtained by means of experimental results, the relaxation effect is generally embedded in the 4R method.

The investigation could be improved by taking the weld and joint geometries more precisely into account and by enhancing the residual stress measurements. In the current work, a simple fillet weld toe radius of $r = 1$ mm was used for the ASW- and HFMI-treated joints as proposed in [12, 14, 33]. Furthermore, Leitner et al. [37] have shown that the beneficial effect of HFMI treatment depends more on the compressive residual stress than the improved weld toe geometry. This simplification can be also justified owing to the formation of microcracks and folding phenomena, and by the fact that the peening creates an undercut type radius (Fig. 9b) at the weld toe, which creates a higher concentration than the fillet-type radius. The effect can be compensated by using a smaller fillet radius. This simplification needs more investigation, because designers prefer to avoid model undercuts when the ENS approach is employed. Nevertheless, if weld toe geometry is improved by means of modified welding technique or post-weld treatments, such as burr grinding and TIG dressing, the improved geometrical weld toe quality (r_{true}) should be considered.

In addition, the material parameters could be defined and fixed with more sophistication. However, this basic version with minimal adjustment seems to work quite well, and the method seems a promising approach for an easy way to enhance design accuracy, especially in the case of higher strength steels.

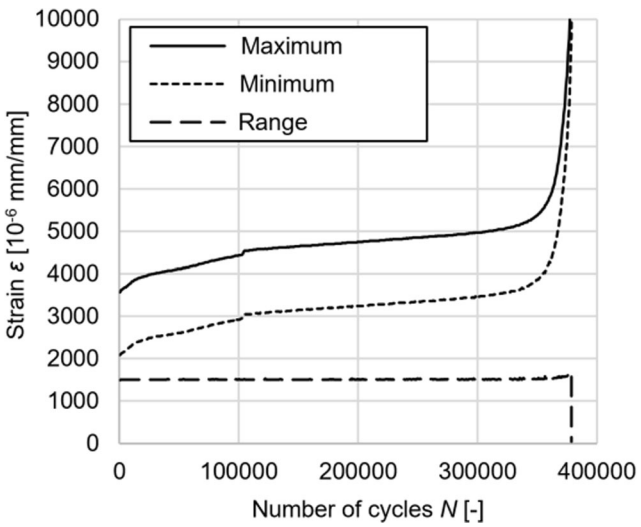

Fig. 18 Strain values during a test in 2507

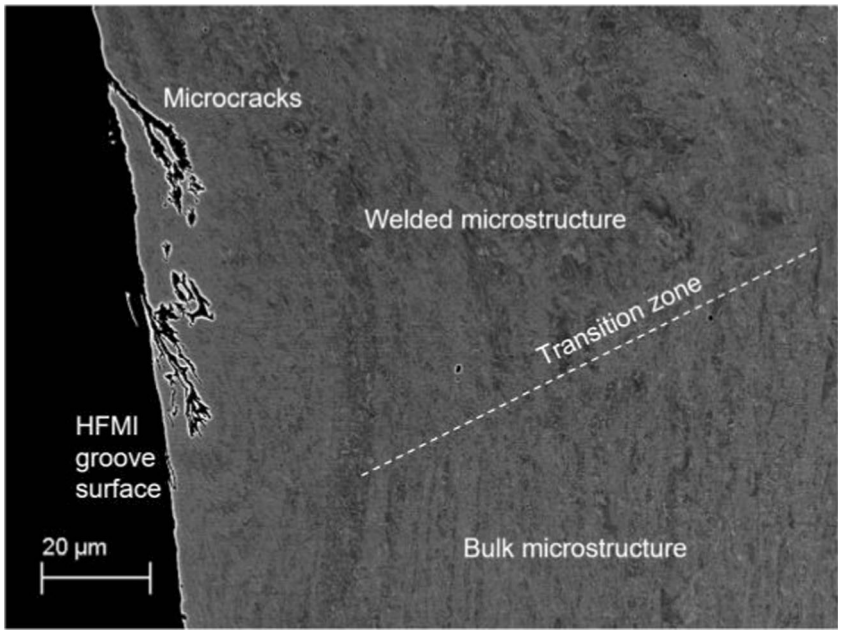

Fig. 19 Cross section of the HFMI groove of a non-fatigued sample showing microcracks close to the transition zone of the weld and bulk material

Metallurgical investigations revealed that the HFMI groove surface contained defects and geometrical discontinuities, like microcracks and folds as illustrated in a scanning electron microscope image of the HFMI groove in Fig. 19. The HFMI treatment was applied using The microcracks were typically in 45° angle to the surface indicating shearing of the material. In many observed cross-sections, these microcracks were found close to the transition zone of the weld and the bulk material, although cracking also existed randomly along the cross-sections of the HFMI grooves. The reason for the microcracks could be the high deformation of the HFMI combined with the high strength of the material and the two-phase microstructure in which the phases have different mechanical properties, which can make the accommodation of high strains difficult.

Of the pre-existing flaw population of the super-duplex 2507 groove surface, the ones in the vicinity of the coarse-grained ferrite in the heat-affected zone were the most prone to initiate a fatigue crack. This was a typical location for the fatigue cracks. Figure 20 shows an example of such a crack

Fig. 20 A secondary crack that has grown in the coarse-grained ferrite phase of an X-joint in 2507

in an X-joint. The presence of the defects could be one contributing factor to the observation that for super-duplex the HFMI treatment did not improve the fatigue strength. The assessment of proper parameters for HFMI of duplex and super-duplex stainless steels needs future investigations.

7 Conclusions

In this paper, the fatigue strength properties of duplex and super-duplex steels were investigated in terms of the conventional S-N approaches and by using the novel 4R method. Based on experimental tests and subsequent analyses, the following conclusions can be drawn:

- The fatigue performance of welded joints made of duplex and super-duplex steels is good.
- Post-weld treatment by HFMI improved the fatigue strength, but only with low stress ratios.
- Fatigue cracks initiated preferentially at the coarse-grained ferrite in the heat-affected zone.
- The HFMI treatment generated, especially in the super-duplex stainless steel, microcracks and folds, which facilitate fatigue crack initiation, and which may be a contributing factor to the limited ability of the HFMI method to provide improvements in high stress ratio fatigue.
- The new 4R method seems to be also applicable for fatigue analysis of duplex and super-duplex steels. By adopting the 4R approach, it is possible to incorporate the strength of a material and the effects of post-weld treatment techniques into fatigue strength calculations.

Acknowledgements The authors wish to thank Outotec, DIMECC Ltd., and the Finnish Funding Agency for Innovation (TEKES) for funding through the BSA (Breakthrough Steels and Applications) program that enabled this research work to be completed.

References

1. Maddox SJ, Manteghi S (2002) Fatigue tests on duplex stainless steel tubular T-joints. Weld World 46:12–19. https://doi.org/10.1007/BF03266367
2. Infante V, Branco CM, Martins R (2003) A fracture mechanics analysis on the fatigue behaviour of cruciform joints of duplex stainless steel. Fatigue Fract Eng Mater Struct 26:791–810. https://doi.org/10.1046/j.1460-2695.2003.00681.x
3. European Commission (2007) Improving the fatigue performance of welded stainless steels. Final report for contract No. 7210-PR/303
4. Baptista R, Infante V, Branco CM (2008) Study of the fatigue behavior in welded joints of stainless steels treated by weld toe grinding and subjected to salt water corrosion. Int J Fatigue 30:453–462. https://doi.org/10.1016/j.ijfatigue.2007.04.011
5. Marquis GB, Maddox SJ (2009) Post-weld fatigue improvement technologies for stainless steel welds. In: Vuori S, Rintamaa R (eds) 20th Int. Conf. Struct. Mech. React. Technol. (SMiRT 20). VTT, Espoo, pp 411–418
6. Kurzydłowski KJ, Matysiak H, Nowacki J, Zając P (2013) Fatigue strength of butt joints welded from duplex steel. Weld Int 27:323–330. https://doi.org/10.1080/09507116.2011.600038
7. EN 1993-1-9 (2005) Eurocode 3 - design of steel structures - part 1–9: Fatigue
8. EN 1993-1-4 (2006) Eurocode 3 - design of steel structures - part 1–4: general rules. Supplementary rules for stainless steels
9. Hobbacher A (2016) Recommendations for fatigue design of welded joints and components, 2nd edn. Springer International Publishing, Cham
10. DNVGL-RP-C203 (2016) Fatigue design of offshore steel structures
11. BS7608:2014 +A1:2015 (2015) Guide to fatigue design and assessment of steel products
12. Nykänen T, Björk T, Laitinen R (2012) Fatigue strength prediction of ultra high strength steel butt-welded joints. Fatigue Fract Eng Mater Struct 36:469–482. https://doi.org/10.1111/ffe.12015
13. Nykänen T, Björk T (2015) Assessment of fatigue strength of steel butt-welded joints in as-welded condition - alternative approaches for curve fitting and mean stress effect analysis. Mar Struct 44:288–310. https://doi.org/10.1016/j.marstruc.2015.09.005
14. Nykänen T, Björk T (2016) A new proposal for assessment of the fatigue strength of steel butt-welded joints improved by peening (HFMI) under constant amplitude tensile loading. Fatigue Fract Eng Mater Struct 39:566–582. https://doi.org/10.1111/ffe.12377
15. Nykänen T, Mettänen H, Björk T, Ahola A (2017) Fatigue assessment of welded joints under variable amplitude loading using a novel notch stress approach. Int J Fatigue 101:177–191. https://doi.org/10.1016/j.ijfatigue.2016.12.031
16. Peippo J, Björk T, Nykänen T (2018) A novel method for fatigue assessment of steel plates with thermally cut edges. Weld World 62:105–115. https://doi.org/10.1007/s40194-017-0529-7
17. Ahola A, Nykänen T, Björk T (2017) Effect of loading type on the fatigue strength of asymmetric and symmetric transverse non-load carrying attachments. Fatigue Fract Eng Mater Struct 40:670–682. https://doi.org/10.1111/ffe.12531
18. Ushirokawa O, Nakayama E (1983) Stress concentration factor at welded joints (in Japanese). Technical report. Ishikwajima-Harima Gihou
19. Anthes RJ, Köttgen VB, Seeger T (1993) Stress concentration factors for butt joints and double T-joints (in German). Schweißen und Scheiden 45:685–688
20. Brennan FP, Peleties P, Hellier AK (2000) Predicting weld toe stress concentration factors for T and skewed T-joint plate connections. Int J Fatigue 22:573–584. https://doi.org/10.1016/S0142-1123(00)00031-1
21. Dabiri M, Ghafouri M, Rohani Raftar HR, Björk T (2017) Neural network-based assessment of the stress concentration factor in a T-welded joint. J Constr Steel Res 128:567–578. https://doi.org/10.1016/j.jcsr.2016.09.024
22. Dabiri M, Ghafouri M, Rohani Raftar HR, Björk T (2017) Utilizing artificial neural networks for stress concentration factor calculation in butt welds. J Constr Steel Res 138:488–498. https://doi.org/10.1016/j.jcsr.2017.08.009
23. Neuber H (1961) Theory of stress concentration for shear-strained prismatical bodies with arbitrary nonlinear stress-strain law. J Appl Mech 28:544–550
24. Masing G (1926) Eigenspannungen und Verfestigung beim Messing. In: Proc. Int. Congr. Appl. Mech. p 332–335
25. Deming WE (1943) Statistical adjustment of data. Dover Publication Inc.
26. Elga (2013) Cromacore DW 329A Duplex. http://www.elga.se/consumables/product/index/category/FLUXCOREDARCWELDING %28FCAW%29/sub-category/

Stainless Steel/product/Cromacore DW329ADuplex. Accessed 9 May 2017
27. Welding Alloys Group (2017) Duplex and superduplex stainless steels. http://www.welding-alloys.com/EN/products-services/welding-alloys-consumables/joining-cored-wires/duplex-and-superduplex-stainless-steels.html. Accessed 8 May 2017
28. Outokumpu (2013) Duplex stainless steel. http://www.outokumpu.com/sitecollectiondocuments/outokumpu-duplex-stainless-steel-data-sheet.pdf. Accessed 5 May 2017
29. Dynatec (2018) HiFIT (High Frequency Impact Treatment). Accessed 12 September 2018
30. Marquis GB, Barsoum Z (2016) IIW Recommendations for the HFMI Treatment - for improving the fatigue strength of welded joints. doi:https://doi.org/10.1007/978-981-10-2504-4
31. Mattila M (2016) Investigation of the fatigue performance of welded duplex stainless steel. Master's thesis. Lappeenranta University of technology
32. Salo J (2016) Fatigue strength of welded joints in super-duplex stainless steel. Master's thesis. Lappeenranta University of technology
33. Yildirim HC (2014) Fatigue strength assessment of HFMI-treated butt welds by the effective notch stress method. Weld World 58: 279–288. https://doi.org/10.1007/s40194-014-0113-3
34. Radaj D, Sonsino CM, Fricke W (2006) Fatigue assessment of welded joints by local approaches, 2nd edition. Woodhead Publishing, Cambridge
35. Stephens RI, Fatemi A, Stephens RR, Fuchs HO (2000) Metal fatigue in engineering, 2nd edition. Wiley
36. Dowling NE (2006) Mechanical Behavior of Materials. Engineering Methods for Deformation, Fracture, and Fatigue. Prentice Hall
37. Leitner M, Mössler W, Putz A, Stoschka M (2015) Effect of post-weld heat treatment on the fatigue strength of HFMI-treated mild steel joints. Weld World 59:861–873. https://doi.org/10.1007/s40194-015-0265-9